https://doi.org/10.5194/hess-2023-54
Preprint. Discussion started: 28 March 2023

Hydrology and Earth System Sciences
Discussions

Technical note: Removing dynamic sea-level influences from groundwater-level measurements

Patrick Haehnel[1], Todd C. Rasmussen[2], and Gabriel C. Rau[3]

[1]Hydrogeology and Landscape Hydrology, Institute of Biology and Environmental Sciences, Carl von Ossietzky University Oldenburg, Ammerländer Heerstraße 114-118, 26129 Oldenburg, Lower Saxony, Germany
[2]Warnell School of Forestry and Natural Resources, University of Georgia, Athens GA, 30602-2152, USA
[3]School of Environmental and Life Sciences, The University of Newcastle, Callaghan, 2238, New South Wales, Australia

Correspondence: Patrick Haehnel (patrick.haehnel@uni-oldenburg.de)

Abstract. The sustainability of limited freshwater resources in coastal settings requires an understanding of the processes that affect them. This is especially relevant for freshwater lenses of oceanic islands. Yet, these processes are often obscured by dynamic oceanic water levels that change over a range of time scales. We use regression deconvolution to estimate an *Oceanic Response Function* (ORF) that accounts for how sea-level fluctuations affect measured groundwater levels, thus providing a clearer understanding of recharge and withdrawal processes. The method is demonstrated using sea-level and groundwater-level measurements on the island of Norderney in the North Sea (Northwest Germany). We expect that the method is suitable for any coastal groundwater system where it is important to understand processes that affect freshwater lenses or other coastal freshwater resources.

1 Introduction

Groundwater is often the dominant source of freshwater on oceanic islands, and the sustainable management of this resource relies on understanding the gains (recharge) and losses (discharge, withdrawals) that are a function of the dynamic forces that act upon it (White and Falkland, 2009). Because freshwater on oceanic islands typically occurs as a lens above denser seawater (Underwood et al., 1992), groundwater withdrawals alter fluid pressures and affect the interface between these fluids. Excessive groundwater extraction can lead to aquifer salinization due to horizontal seawater intrusion as well as vertical upconing (Barlow, 2003; Falkland and Custodio, 1991). Thus, island groundwater resources are among the most vulnerable in the world, stressing the need for their careful monitoring and understanding to sustain their productivity (White and Falkland, 2009).

Estimating groundwater recharge on oceanic islands is challenging because groundwater levels in such systems are highly dynamic and can be influenced by multiple factors, such as periodic and aperiodic sea-level changes, coastal morphology, aquifer properties, precipitation, and withdrawals (Jiao and Post, 2019), that interact to influence near-shore groundwater levels (e.g., Patton et al., 2021). Several methods have been used for estimating groundwater recharge, such as lysimeters (e.g., Stuyfzand, 2017), tritium-helium age dating (e.g., Houben et al., 2014; Röper et al., 2012), and stable-isotope methods (e.g., ^{18}O, ^{2}H, see Koeniger et al., 2016; Post et al., 2022). However, temporal differentiation of the recharge, that is critical for understanding the dynamics of coastal groundwater systems, is costly and time intensive using these methods.

https://doi.org/10.5194/hess-2023-54
Preprint. Discussion started: 28 March 2023


Hydrology and Earth System Sciences
Discussions

Regression deconvolution provides an alternative method for quantifying groundwater processes using real-time, groundwater-level measurements. The method has been successfully applied to remove the influence of barometric pressure (Furbish, 1991; Rasmussen and Crawford, 1997), Earth tides (Toll and Rasmussen, 2007), near-surface water content (Rasmussen and Mote, 2007), and river stages (Spane and Mackley, 2011) from groundwater time series. Yet, despite its versatility, applications using convolution methods are commonly missing from hydrogeology textbooks (Olsthoorn, 2008). In addition, (to the authors' knowledge) convolution has not been used to remove sea-level influences from dynamic groundwater levels in coastal settings where periodic and aperiodic influences often obscure important groundwater processes, such as recharge and pumping.

The objective of this work is to demonstrate the use of regression deconvolution for removing sea-level influences on groundwater-level measurements in an unconfined coastal aquifer consisting of unconsolidated sediments. The application uses groundwater-level, sea-level, and meteorologic data collected on the coastal island of Norderney, located in Northwest Germany in the North Sea. We believe that our method is suitable for application in other coastal aquifers to support their sustainable management by better understanding the processes within – and physical characteristics of – freshwater lenses.

2 Influences on coastal groundwater levels

2.1 Conceptual overview

Figure 1 presents our conceptual model of the influence of sea levels on groundwater in coastal islands. Note that a freshwater lens is present above an underlying saltwater zone, where the depth to the freshwater-saltwater interface is a function of the water table elevation above mean sea level, as defined by the Ghyben-Herzberg principle (Jiao and Post, 2019; Post et al., 2018).

Barometric influences within unconfined aquifers are a function of the depth of the water table below the ground surface and the air diffusivity within the unsaturated zone (Rasmussen and Crawford, 1997). Barometric pressure displays diurnal fluctuations due to solar heating, along with seasonal and weather-related forcing (McMillan et al., 2019). Sea-level variation is dominated by diurnal and semi-diurnal periodicities, along with aperiodic behavior resulting from storm events (Boon, 2011).

The influence of fluctuating sea levels diminishes with distance from the shoreline, with tidal variations attenuating more rapidly than intra- (e.g., seasonal) and inter-annual (e.g., extreme events, such as floods and droughts) variation (Ferris, 1952; Li et al., 2004; Nielsen, 1990). Precipitation recharges groundwater by vertical percolation through the overlying unsaturated zone or by direct recharge from surface-water bodies that fill during storm events.

2.2 Single-factor regression deconvolution

Barometric-pressure changes often influence groundwater levels in both confined and unconfined aquifers. The barometric efficiency (BE) is commonly used to describe the instantaneous linear relationship between discrete changes in barometric-pressure $\Delta\mathrm{BP}$ and groundwater-level responses $\Delta\mathrm{GW}$ (Rasmussen and Crawford, 1997):

$$\mathrm{BE} = -\frac{\Delta\mathrm{GW}}{\Delta\mathrm{BP}}. \tag{1}$$

https://doi.org/10.5194/hess-2023-54
Preprint. Discussion started: 28 March 2023

Hydrology and Earth System Sciences
Discussions
Open Access
EGU

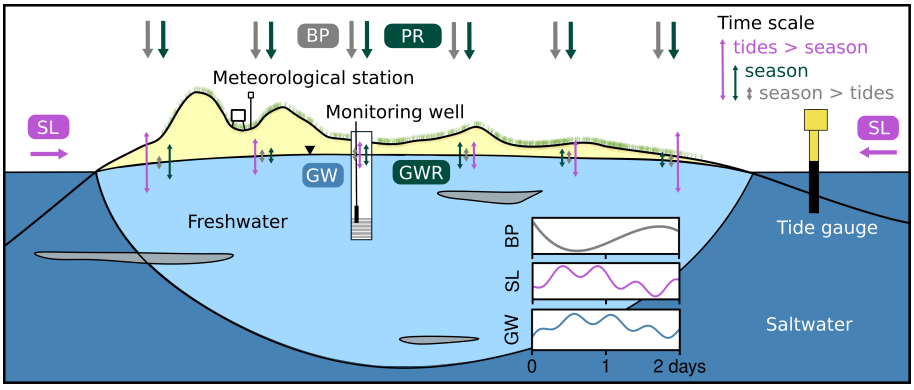

Figure 1. Conceptual model of groundwater-level fluctuations (GW) on a coastal island with barometric-pressure (BP), sea-level (SL), and groundwater-recharge (GWR) forcing. The latter results from precipitation (PR) on oceanic islands. Note that the amplitude of groundwater fluctuations is larger for tidal influences near the shoreline than seasonal influences, but smaller toward the center of the island. The left-hand side of the island constitutes the seaward side, while the right-hand side constitutes the leeward side of the island. Seasonal influences diminish on the leeward side of the island.

While groundwater responses to barometric-pressure changes are frequently assumed to be instantaneous, there is often a delayed response that depends upon the degree of confinement, depth to the water table, borehole-storage effects, whether the borehole is open or sealed, and whether an absolute or relative (gauge) pressure sensor is used (Rojstaczer and Riley, 1990; Rasmussen and Crawford, 1997).

Response functions $\beta(\tau)$ are commonly used to quantify the time-lagged response caused by an impulse input $x(t)$ to the output time series $y(t)$ using the convolution operator $\star$

$$y(t) = \beta(\tau) \star x(t) = \sum_{k=0}^{K} \beta(\tau_k)\, x(t - \tau_k), \tag{2}$$

where K is the maximum number of time lags, t is the observation time, and $\tau_k = k\,\Delta t$ is the time lag between the input and the observed response, with sampling interval Δt (Rasmussen and Mote, 2007; Rau et al., 2020). We define $m = \tau_K$, which is the maximum time lag or memory of the system beyond which the output is unaffected by an input (Rasmussen and Mote, 2007). Convolution assumes a linear, time-invariant system, with responses to individual inputs being independent of other inputs.

While convolution is used to find the output function $y(t)$ as a function of the response function $\beta(\tau)$ and the input function $x(t)$, we are often interested in finding the response function by inversion of the input and output time series using the deconvolution operator $\backslash$ (i.e., backslash)

$$\beta(\tau) = x(t) \backslash y(t). \tag{3}$$

Deconvolution can be implemented using multiple regression by forming a set of linear equations

$$y(t) = \beta(\tau_0)\, x(t - \tau_0) + \beta(\tau_1)\, x(t - \tau_1) + \cdots + \beta(\tau_K)\, x(t - \tau_K), \tag{4}$$

https://doi.org/10.5194/hess-2023-54
Preprint. Discussion started: 28 March 2023


Hydrology and Earth System Sciences
Discussions

where the left-hand side are the observed outputs and the right-hand side consists of the unknown response function values and lagged input values (Toll and Rasmussen, 2007). This equation is written in matrix form as

$$\boldsymbol{y} = \boldsymbol{\beta}\,\mathbf{X}, \tag{5}$$

where $\boldsymbol{y}$ is the $[1 \times n]$ row vector of n observed outputs, $\boldsymbol{\beta}$ is the $[1 \times m]$ row vector of unknown response coefficients, and $\mathbf{X}$ is the $[m \times n]$ matrix of observed inputs, with each row lagged by one time unit. Note that the first m columns of $\boldsymbol{y}$ and $\mathbf{X}$ must be omitted unless prior input data are available; i.e., observations may be lacking for $x(t-m)$.

The resulting matrix equation can be solved using ordinary least-squares (OLS) regression, which takes the matrix form

$$\hat{\boldsymbol{\beta}} = \mathbf{X} \setminus \boldsymbol{y} = \boldsymbol{y}\mathbf{X}^{\mathrm{T}} \left[\mathbf{X}\mathbf{X}^{\mathrm{T}}\right]^{-1}, \tag{6}$$

where the superscripts $[\cdot]^{\mathrm{T}}$ and $[\cdot]^{-1}$ indicate the matrix transpose and inverse, respectively, and where alternative matrix solvers are likely to be more efficient and accurate. The reconstructed (fitted) time series, $\hat{\boldsymbol{y}} = \hat{\boldsymbol{\beta}}\,\mathbf{X}$, can then be used to find the residual, as well as a time series that is corrected from the process influence as follows

$$\boldsymbol{y}_c = \boldsymbol{y} - \hat{\boldsymbol{y}} = \boldsymbol{y} - \hat{\boldsymbol{\beta}}\,\mathbf{X}. \tag{7}$$

It is recommended to perform the deconvolution using the first differences of the measurements, leading to Eq. 5 becoming

$$\Delta\boldsymbol{y} = \boldsymbol{\beta}\,\Delta\mathbf{X}. \tag{8}$$

This removes the effect of persistent trends in the data and therefore avoids a bias in the regression (Rasmussen and Crawford, 1997; Butler Jr. et al., 2011). To avoid spurious influences from the fact that the reconstruction hinges on an initial groundwater measurement that cannot be corrected, we recommend that the mean of the corrected time series is matched to the uncorrected one.

2.3 Multi-factor regression deconvolution

Toll and Rasmussen (2007) and Butler Jr. et al. (2011) presented a method to analyze and remove both barometric pressure and Earth tides (i.e., two independent processes) from groundwater levels. This procedure can be extended to account for multiple drivers as follows

$$\Delta Y(t) = \sum_{p=1}^{P} \sum_{k=0}^{K^p} \beta^p(\tau_k)\,\Delta X^p(t-\tau_k). \tag{9}$$

Here, ΔX^p is the time series of the differences of influencing process p; P represents the total number of processes; $\beta^p(\tau_k)$ represents the time-lagged impulse response function coefficients for process p; $m^p = \tau_{K^p}$ is the total memory for process p. Note that all processes propagate through the subsurface either vertically or horizontally, and are increasingly attenuated and time-lagged with distance from their origin. This approach allows us to consider multiple dynamic processes that could affect groundwater levels, including precipitation, evapotranspiration, barometric pressure, streamflow, Earth tides, soil moisture, etc. Note that process-based indices are always notated as superscripts here.

https://doi.org/10.5194/hess-2023-54
Preprint. Discussion started: 28 March 2023

Hydrology and Earth System Sciences
Discussions

2.4 Process response functions and time series correction

The response function for a process is determined from the impulse responses (Eq. 6) as follows

$$B^p(\tau_k) = \sum_{k=0}^{K^p} \hat{\beta}^p(\tau_k). \tag{10}$$

Note that we state the process response function B^p as a generic term that allows disentanglement of multiple processes p each with total memory m^p. For example, the *Barometric Response Function* (BRF) is determined by taking the cumulative sum of the impulse responses to barometric pressure, $\hat{\beta}^{BP}$ (Rasmussen and Crawford, 1997)

$$\mathrm{BRF}(\tau_k) = \sum_{k=0}^{K^{\mathrm{BP}}} \hat{\beta}^{\mathrm{BP}}(\tau_k). \tag{11}$$

Analogously, an *Earth Tide Response Function* (ETRF) as well as a *River Response Function* (RRF) can be formulated in the same way. These influences have successfully been used to characterise subsurface processes and properties and to correct groundwater levels from the respective influences (e.g., Spane, 2002; Toll and Rasmussen, 2007; Butler Jr. et al., 2011; Spane and Mackley, 2011; Rau et al., 2020). Here, we note that despite being used to correct groundwater levels, the name ETRF has not explicitly been defined in the literature.

The aim of this work is to illustrate how regression deconvolution can be used to estimate the *Oceanic Response Function* (ORF)

$$\mathrm{ORF}(\tau_k) = \sum_{k=0}^{K^{\mathrm{SL}}} \hat{\beta}^{\mathrm{SL}}(\tau_k). \tag{12}$$

This characterises the effects of sea-level fluctuations $\mathrm{SL}(t)$ on measured groundwater levels

$$\mathrm{GW}(t) = \mathrm{ORF}(m^{\mathrm{SL}}) \star \mathrm{SL}(t), \tag{13}$$

with sea-level memory m^{SL}. We note that our approach employs multi-factor regression deconvolution to disentangle the simultaneous influences of sea levels and barometric pressure on observed groundwater levels, so $\Delta \boldsymbol{x} = \{\Delta\mathrm{SL}, \Delta\mathrm{BP}\}$. We did not analyze Earth-tide responses, as they are generally negligible in unconfined finite-depth aquifers made of unconsolidated sediment (Rojstaczer and Riley, 1990). The formulated correction procedure yields corrected groundwater levels

$$GW_c(t) = GW(t) - \sum_{p=1}^{P} \sum_{k=0}^{K^p} \hat{\beta}^p(\tau_k)\, \Delta X^p(t_i - \tau_k). \tag{14}$$

Again, the mean of the corrected values must be matched to the mean of the uncorrected values (as explained earlier).

3 Application

3.1 Field site, monitoring, and data processing

Norderney is a coastal barrier island that is part of the East Frisian island chain located in the North Sea near the Northwest German coast (Fig. 2). The island covers an area of about 25 km^2, with an east-to-west extent of 14 km and an average

https://doi.org/10.5194/hess-2023-54
Preprint. Discussion started: 28 March 2023

Hydrology and Earth System Sciences
Discussions
Open Access
EGU

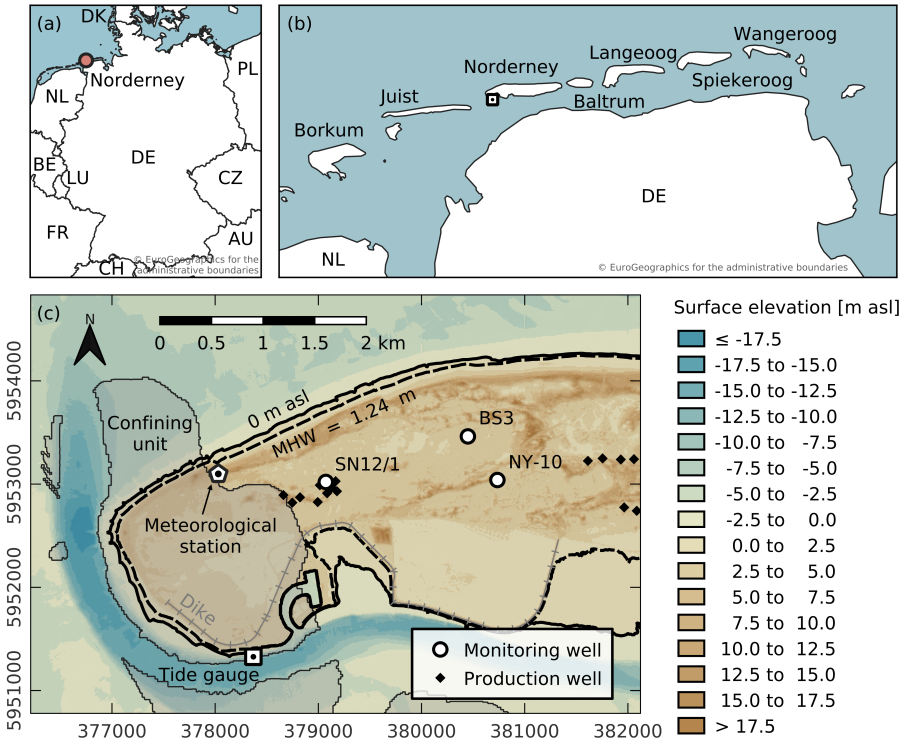

Figure 2. Map of Norderney Island in Northwest Germany showing three monitoring wells, production wells, tide gauge, meteorologic station, and a confining unit (shaded area) to the west. Mean high water (MHW) is the average between 2010 and 2020 from (WSA Ems-Nordsee, 2021). Coordinate reference system is UTM Zone 32N (EPSG:25832). Data sources: EuroGeographics and UN-FAO (2020), © EuroGeographics for the administrative boundaries; Haehnel et al. (under review); Niedersächsischer Landesbetrieb für Wasserwirtschaft, Küsten- und Naturschutz (NLWKN) [Lower Saxony State Agency for Water Management, Coastal and Nature Conservation] (2021); Sievers et al. (2020); Stadtwerke Norderney (2021); WSA Ems-Nordsee (2021).

north-to-south extent of 2 km (Naumann, 2005; Streif, 1990). Rainfall is the only source of freshwater on the island, and 782 mm of precipitation were observed during our one-year research period (1 November 2018 to 31 October 2019) at the Norderney meteorological station (DWD Climate Data Center (CDC), 2021a). Approximately half of the island's precipitation was estimated to recharge the aquifer (Naumann, 2005).

Semi-diurnal tides dominate Norderney sea-level fluctuations. For our research period, the mean high water (MHW) was 1.26 m asl (above sea level), and the mean low water (MLW) was -1.18 m asl (Wasserstraßen- und Schifffahrtsamt Ems-Nordsee (WSA Ems-Nordsee) [Waterways and Shipping Authority Ems-North Sea], 2021), which yields a tidal range of 2.44 m that corresponds to meso-tidal conditions (Hayes, 1979). Seasonal flooding typically occurs during the autumn and winter seasons (Holt et al., 2019), and is defined using a sea level 1.5 m above MHW for the region (Gönnert, 2003). The maximum sea level during our study period was 3.03 m asl (1.77 m above MHW) on 8 January 2019 (WSA Ems-Nordsee, 2021).

https://doi.org/10.5194/hess-2023-54
Preprint. Discussion started: 28 March 2023

Hydrology and Earth System Sciences
Discussions

Table 1. Reference data for groundwater monitoring wells (Stadtwerke Norderney, 2021). Coordinate reference system is UTM Zone 32N (EPSG:25832).

	Well name		
	BS3	NY-10	SN12/1
Latitude [°N]	53.716	53.712	53.712
Longitude [°E]	7.188	7.193	7.168
Northing [m]	5 953 462	5 953 039	5 953 021
Easting [m]	380 449	380 736	379 073
Ground surface elevation [m asl]	2.50	2.83	4.48
Top of screen [m asl]	-4.68	-3.57	-18.02
Bottom of screen [m asl]	-6.98	-4.57	-20.02
Screen length [m]	2	1	2
Casing diameter [cm]	5	5	5
Distance to 0 m asl [m][a]	741	1154	688
Distance to MHW [m][b]	692	978	456
Distance to production well [m][c]	1187	896	39

[a]Minimum Euclidean distance to 0 m asl contour using DEM of Sievers et al. (2020).
[b]Minimum Euclidean distance to mean high water (MHW) contour (1.24 m asl, average between 2010 and 2020 from WSA Ems-Nordsee (2021)) using DEM of Sievers et al. (2020).
[c]Euclidean distance to closest production well.

The island's geomorphology is characterized by beaches and dunes on the seaward north, and salt marshes and back-barrier tidal flats on the leeward south (Petersen et al., 2003). Holocene dune sediments are composed of fine-grained sands and sand flat with mixed flat deposits, extending to about 30 to 40 m bsl (below sea level) in the central part of the island (Naumann, 2005; Streif, 1990). These sediments extend to a depth of about 10 m bsl below the western part of the island, where they transition to a confining unit of Holocene clay, silt, and basal peat (Schaumann et al., 2021), shown in Fig. 2c. Mud flat deposits are present locally below the central part of the island (Naumann, 2005). Pleistocene sandy deposits are found below Holocene sediments, which largely originated from Drenthian sandur-type plains (Naumann, 2005; Schaumann et al., 2021).

A more detailed summary of the island's development, geomorphology, geology, and hydrogeology can be found in Haehnel et al. (under review). Schaumann et al. (2021) described the Holocene and Pleistocene geology in detail, and Karle et al. (2021) reconstructed the Holocene landscape development of the area during sea-level transgression.

Hourly groundwater levels are routinely collected by the Municipal Works Norderney using STS DL/N 70 dataloggers in open (uncapped) monitoring wells (Stadtwerke Norderney [Municipal Works Norderney], 2021). This study focuses on a subset of these wells (SN12/1, BS3, NY-10) for the one-year period between 1 November 2018 and 31 October 2019. As summarized

https://doi.org/10.5194/hess-2023-54
Preprint. Discussion started: 28 March 2023


Hydrology and Earth System Sciences
Discussions

in Table 1, these monitoring wells have short (1 to 2 m) screen lengths. Both BS3 and NY-10 screened zones are shallow, while SN12/1 has a deeper screen from 18 to 20 m bsl, which is below the base elevation of the nearby confining unit (Fig. 2c; Haehnel et al., under review). Both SN12/1 and BS3 are located at similar straight-line distances (688 and 741 m, respectively) to the shoreline (i.e., the 0 m asl contour line), while NY-10 is located more centrally on the island at a greater distance (1154 m) (Table 1). The distance to the MHW contour line is also presented in Table 1 because the shoreline distance is ambiguous when tides are present.

Hourly barometric-pressure and precipitation data were obtained from the meteorological station located near the northwestern shoreline (DWD Climate Data Center (CDC), 2021b). Daily precipitation totals are used for graphical comparison with other variables (DWD Climate Data Center (CDC), 2021a). Sea levels collected at one-minute intervals were obtained from the tide gauge "Norderney Riffgat" (Wasserstraßen- und Schifffahrtsverwaltung des Bundes (WSV) [Federal Waterways and Shipping Administration], 2021), located near the southwestern shoreline. Tidal data were downsampled to hourly intervals for subsequent analysis. An hourly time series of the extracted water volume from the western production well cluster near SN12/1 (Fig. 2c) between 13 and 20 November 2022 was provided by the local water supplier (Stadtwerke Norderney, 2023).

Groundwater and tidal data were inspected prior to analysis and no issues (e.g., gaps, spikes, steps) were found. Barometric-pressure and precipitation data were examined using an automated evaluation and correction procedure by the data provider (DWD Climate Data Center (CDC), 2021a, b). No data are missing in any time series during the research period. All data have time zone UTC+1.

The low-pass finite-impulse-response filter, "LP241H079122kM3" from Shirahata et al. (2016) was applied to groundwater and sea levels for comparison with regression deconvolution results. The filter uses a ten-day symmetric window designed to remove diurnal and semi-diurnal tidal constituents as well as their higher harmonics.

3.2 Processes affecting groundwater levels

Sea-level, barometric-pressure, and daily-precipitation data are presented in Fig. 3a and 3b. Note the aperiodic meteorological as well as the sea-level influences, that are dominated by astronomical tides, on groundwater levels (Fig 3c). This demonstrates the overlapping effects of both vertical propagation of atmospheric effects as well as lateral effects of sea-level variation. Groundwater levels show an oscillating semi-diurnal pattern with differing magnitudes due to sea-level influences that propagate through the aquifer (Fig. 3c) and reflect both periodic as well as aperiodic changes in sea level (e.g., the storm event on 8 January 2019). The well furthest from the shoreline, NY-10, shows the strongest attenuation of the oscillating sea levels, while the attenuation in BS3 and SN12/1 is smaller due to their greater proximity to the shoreline. Yet, BS3 is more strongly attenuated than SN12/1 despite their similar distance to the shoreline. This is likely explained by the nearby confining unit in the west (Fig. 2) that allows the signal to propagate more rapidly due to a smaller storativity.

In addition to changes in sea level, groundwater levels in BS3 and NY-10 show precipitation responses, but these are largely obscured in SN12/1. The precipitation response of BS3 and NY-10 is discernible in mid-August 2019, where groundwater levels increase despite a lack of change in sea levels. Also note that groundwater levels increase while sea levels decrease in late-September 2019.

https://doi.org/10.5194/hess-2023-54
Preprint. Discussion started: 28 March 2023

Hydrology and Earth System Sciences
Discussions

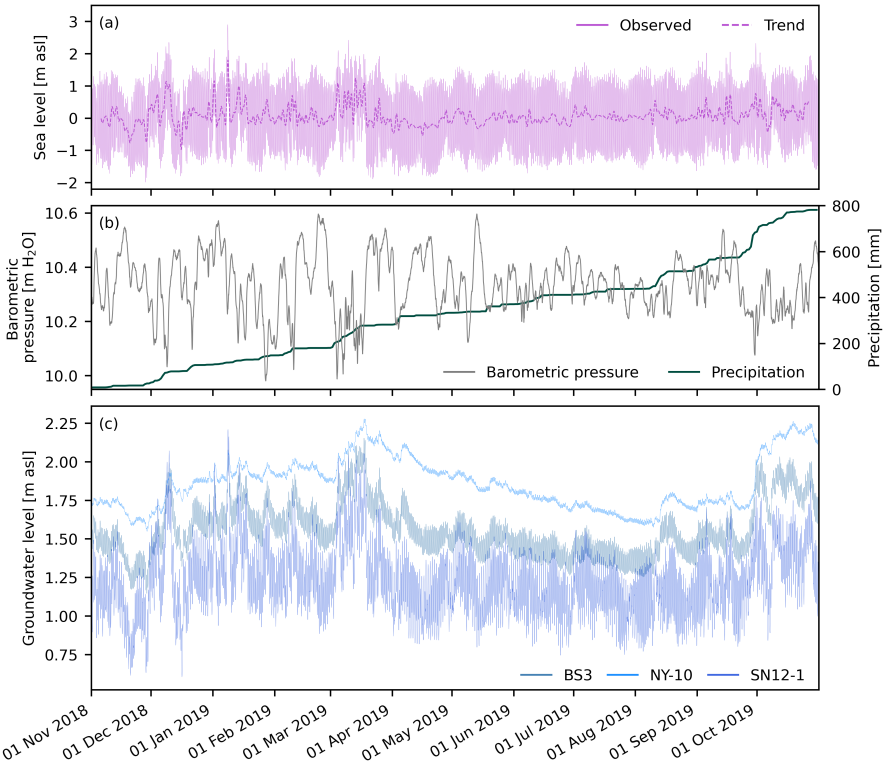

Figure 3. Time series of (a) sea level, (b) barometric pressure and cumulative daily precipitation, and (c) groundwater levels in BS3, NY-10, and SN12/1.

3.3 Removing dynamic sea-level influences

Periodic and aperiodic sea-level fluctuations were removed from groundwater measurements using regression deconvolution (Fig. 4). The simultaneous removal of barometric-pressure influences was tested as well, but instantaneous coefficients $\hat{\beta}^{\mathrm{BP}}$ were insignificant. This is consistent with shallow water tables and high air permeabilities in the sandy surficial deposits that promotes rapid equilibration of aquifer heads (cf, Table 1 and Fig. 3).

The storm event on 8 January 2019 provides an opportunity to evaluate our method. Here, the original groundwater-level time series (Fig 3c) and their trend (Fig. 4) react to the sudden increase in sea level. The corrected time series now shows only a minor response to the storm event with small increase that is likely due to storm-related recharge.

Corrected groundwater levels in BS3 and NY-10 now show contemporaneous responses to precipitation events that increase with increasing precipitation (Fig. 4ab). For example, the precipitation response is now readily observed in early-April 2019, mid-August 2019, and late-September 2019. Note further that corrected groundwater levels remove more of the sea-level influence than filtered trends (e.g., March 2019). The corrected signal now provides a useful tool for examining the duration and magnitude of groundwater recharge.

https://doi.org/10.5194/hess-2023-54
Preprint. Discussion started: 28 March 2023

Hydrology and Earth System Sciences
Discussions

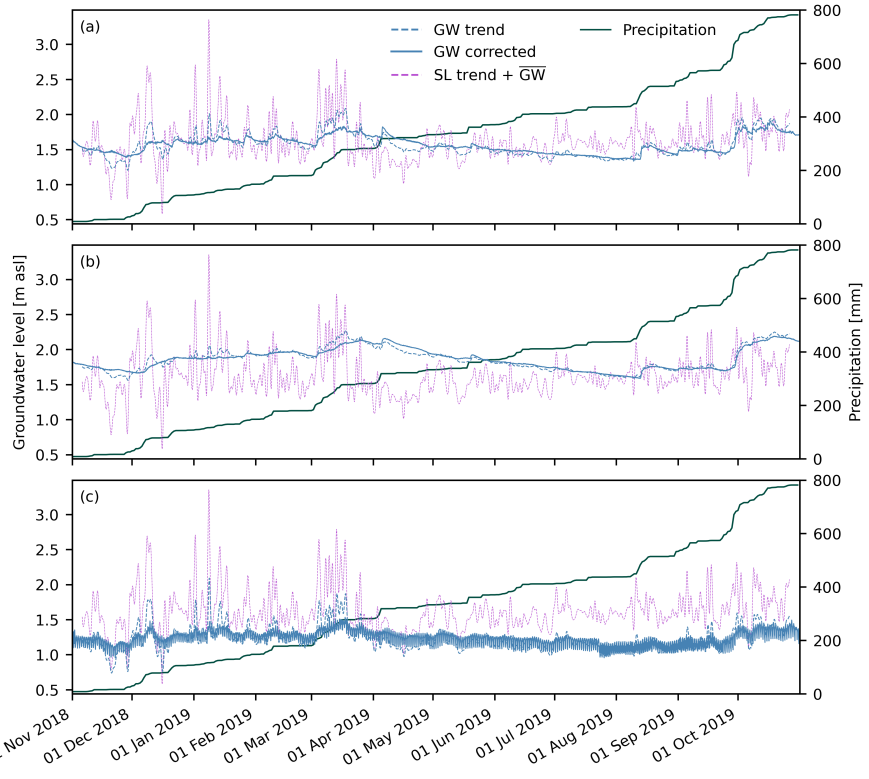

Figure 4. Corrected groundwater levels in (a) BS3, (b) NY-10, and (c) SN12/1 with oceanic response function memories, m^{SL} of 150, 250, and 48 h, respectively. Groundwater and sea-level trends as well as cumulative daily precipitation also shown. The mean groundwater level is added to the sea-level trend time series for easier comparison.

3.4 Oceanic Response Function (ORF)

Figure 5 shows the instantaneous coefficients $\hat{\beta}^{\mathrm{SL}}$ and their cumulative sum that represents the Ocean Response Function (ORF). The coefficients are largest for small time lags and approach zero at longer lag times. Note that values should approach zero as they approach the memory of the system (i.e., sea-level changes no longer influence groundwater levels). Also note that each well has a unique ORF. Similar to the river-stage response function used by Spane and Mackley (2011), this memory should be longer for locations further from the source. The ORF is greater for stronger influences than for weaker influences, which is also a function of the distance to shoreline. Similar to the river-stage response function, the ORF is a function of aquifer hydraulic diffusivity, shoreline distance, beach sediment composition, borehole-storage, and well-skin effects (Spane and Mackley, 2011).

The maximum lag time (i.e., memory) also varies by well, with 150 and 250 h for BS3 and NY-10, respectively, which reflects the greater distance to the shoreline of NY-10. The ORF stabilizes to maximum values of 0.38 and 0.27 for BS3 and NY-10, respectively (Fig. 5ab), again reflecting the distance to the shoreline. The Harmonic Least Squares (HALS) analysis

https://doi.org/10.5194/hess-2023-54
Preprint. Discussion started: 28 March 2023

Hydrology and Earth System Sciences
Discussions
Open Access
EGU

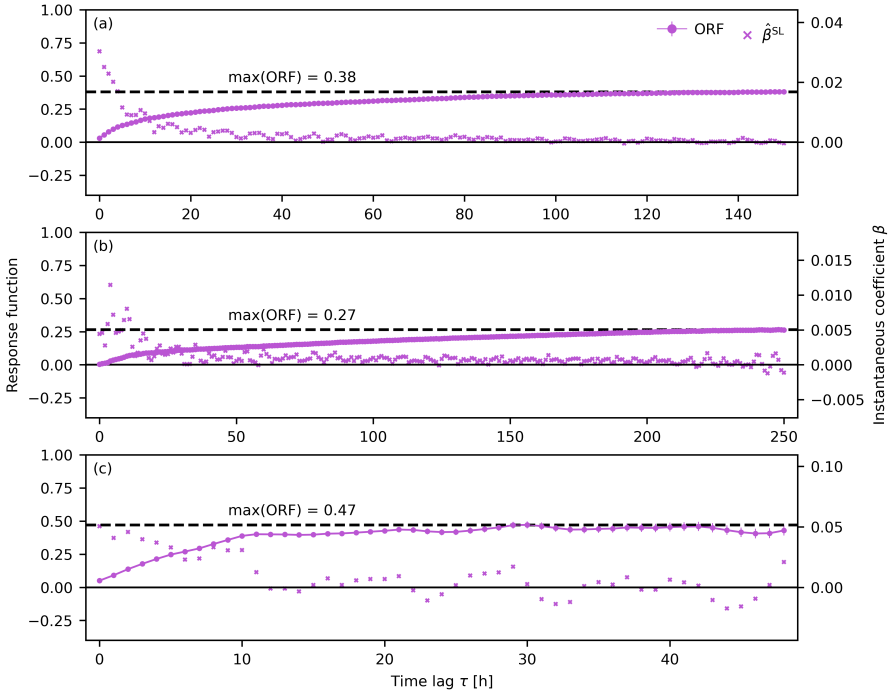

Figure 5. Oceanic Response Function (ORF) for (a) BS3, (b) NY-10, and (c) SN12/1 with with corresponding instantaneous coefficients $\hat{\beta}^{\mathrm{SL}}$. Note the different maximum time lag for each well on the x-axis. Vertical error bars indicate an uncertainty of one standard error for the Oceanic Response Function (Appendix A).

applied to corrected time series with different sea-level memories suggests that ocean tides are removed with small lags, and longer lags are required for aperiodic events (Appendix B).

Well SN12/1 shows a faster response to sea-level changes and the maximum ORF of 0.47 is attained within two days (Fig. 5c), which can be explained by the presence of the nearby confining unit (Fig. 2c). However, corrected groundwater levels still show periodic fluctuations (Fig. 4c) that HALS analysis identified as a diurnal pattern associated with the S_1 tidal constituent that is not removed by deconvolution because it is not present in sea-level observations (Fig. B2c). This S_1 response may be due to meteorological (e.g., evapotranspiration) or other (e.g., groundwater extraction) influences that vary at this frequency.

3.5 Revealing groundwater extraction

Figure 6 shows an eight-day window in November 2018 of observed and sea-level corrected groundwater levels from SN12/1. While the influence of groundwater extraction was masked by sea-level influences, it is clearly present after correction. Groundwater declines in the corrected time series coincide with daily extraction. This explains the visible mixed-tide type present in observed groundwater levels that cannot originate from the semi-diurnal, M_2-dominated ocean tide, with only small diurnal components (cf. Fig. B1).

https://doi.org/10.5194/hess-2023-54
Preprint. Discussion started: 28 March 2023

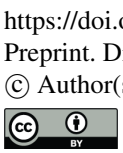

Hydrology and Earth System Sciences
Discussions
Open Access
EGU

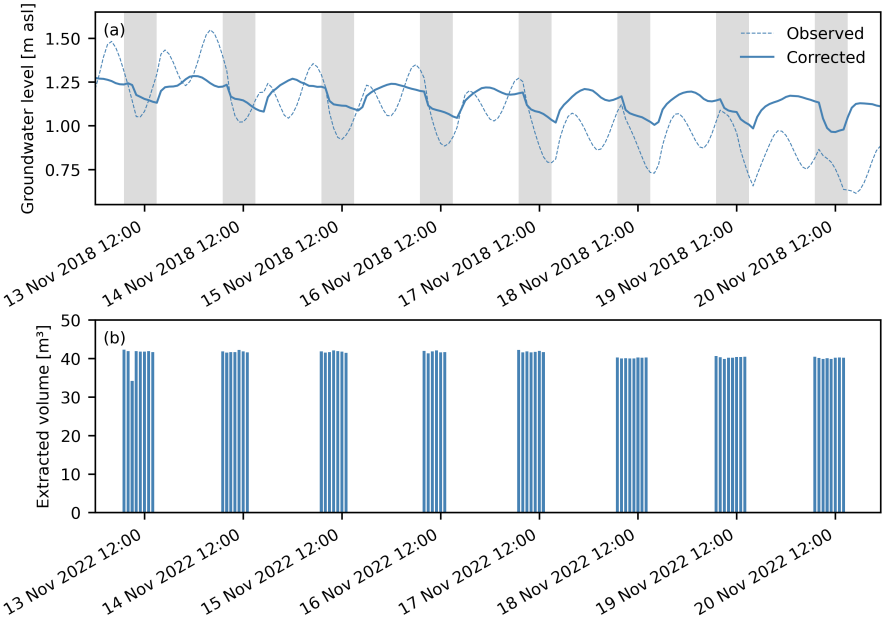

Figure 6. Time series of (a) observed and corrected groundwater levels of SN12/1 and (b) extracted groundwater volume of the production wells around SN12/1 for an eight-day time period. Grey shaded areas in (a) indicate the main extraction time period between 7 AM and 3 PM. Note that the years of both time series differ since no hourly extraction data were available for the studied time frame. However, overall groundwater extraction patterns over a season are generally stable and comparable since the early 2000s (Stadtwerke Norderney, 2021).

We compare this pattern with groundwater extraction data from 2022, which shows that pumping patterns are similar to corrected groundwater levels. We rely on 2022 extraction data because such data were not collected during the study period. Also, seasonal extraction patterns and yearly extraction volumes have remained stable since the early 2000s (Stadtwerke Norderney, 2021). The strong coherence between these two time series provides further evidence for the utility of regression deconvolution for removing interference from external stimuli.

4 Conclusions

We demonstrate how regression deconvolution can be used to remove sea-level influences from groundwater levels measured in coastal aquifers, which has not been illustrated before. We define and use an Oceanic Response Function (ORF) to represent the time lag dependent response coefficients for characterising groundwater responses to sea-level changes. Once sea-level influences have been removed, the resulting groundwater levels clearly show previously masked responses to precipitation and groundwater extraction. In this application, the horizontal propagation of sea-level changes dominates groundwater responses.

Our results add to the suite of potential application of regression deconvolution for characterising and removing external perturbations on groundwater levels, including barometric, Earth tide, river stage, and, now, oceanic changes. Our approach is

https://doi.org/10.5194/hess-2023-54
Preprint. Discussion started: 28 March 2023

Hydrology and Earth System Sciences
Discussions
Open Access
EGU

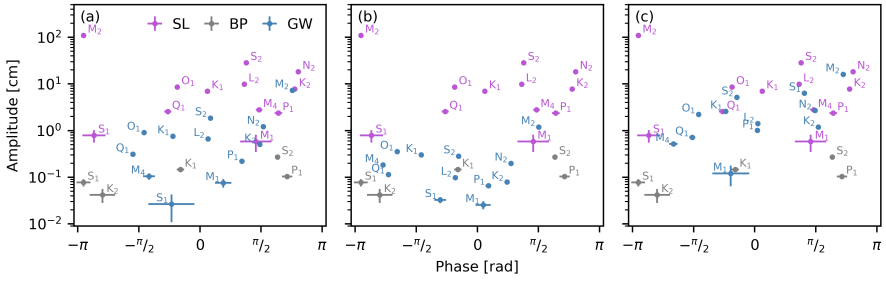

Figure B1. Amplitudes and phases obtained using Harmonic Least Squares (HALS) analysis of groundwater (GW) time series of monitoring wells (a) BS3, (b) NY-10, and (c) SN12/1. Each plot shows the HALS analysis for sea level (SL) and barometric pressure (BP). Error bars show uncertainty of one standard error.

suitable for interpreting data from groundwater monitoring of freshwater resources in oceanic and coastal aquifers, which is useful as it underpins improved investigation and sustainable management of these critical systems. Further research should focus on systematically investigating how Oceanic Response Functions are affected by hydraulic processes and properties in coastal aquifers, as well as estimating the response function associated with groundwater extraction once contemporaneous data are available.

While many hydrogeological settings will likely require the estimation of barometric and other effects (e.g., Earth tides, soil moisture, river stage), we neglect these influences at this site due to their minimal influence. Regardless of the specific application, however, our methodology for removing multiple factors should provide sufficient flexibility for interpreting and removing these influences.

Appendix A: Uncertainty estimation of the response function

The standard error, $\mathrm{SE}_{\mathrm{ORF}}(\tau_k)$, of the ORF at time lag τ_k is calculated from the $[m^{\mathrm{SL}} \times m^{\mathrm{SL}}]$ covariance matrix $\boldsymbol{\sigma}$ for the instantaneous coefficients β^{SL} obtained by regression deconvolution

$$\mathrm{SE}_{\mathrm{ORF}}(\tau_k) = \sqrt{\sum_{i=0}^{k} \sigma_{ii} + 2 \sum_{i=0}^{k} \sum_{j=i}^{k} \sigma_{ij}}, \tag{A1}$$

where σ_{ii} is the variance of instantaneous coefficients $\hat{\beta}^{\mathrm{SL}}$ at time lag τ_i, and σ_{ij} is the covariance at lags τ_i and τ_j.

Appendix B: Harmonic least squares analysis of observed and corrected time series

Amplitudes and phases of major tidal constituents (see e.g., McMillan et al., 2019) were obtained from sea-level and groundwater levels using Harmonic Least Squares (HALS) analysis (for an outline of HALS see e.g., Schweizer et al., 2021). Barometric

https://doi.org/10.5194/hess-2023-54
Preprint. Discussion started: 28 March 2023

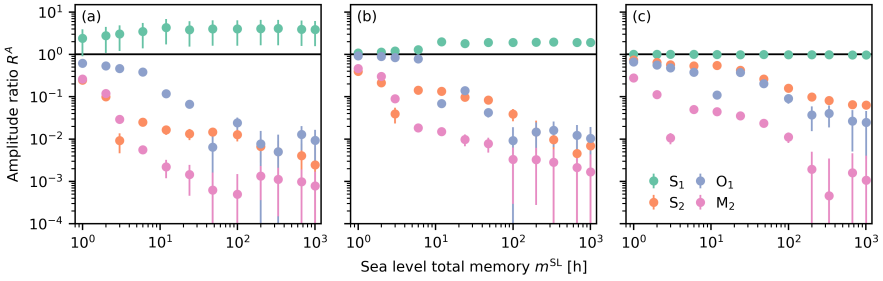

Figure B2. Amplitude ratios of observed and corrected groundwater levels (Eq. (B1)) for tidal constituents obtained by the Harmonic Least Squares (HALS) analysis performed on (a) BS3, (b) NY-10, and (c) SN12/1 as a function of the sea-level memory (m^{SL}). Error bars show uncertainty of one standard error.

pressure was only analyzed for the subset of tidal constituents relevant to atmospheric tides (Rau et al., 2020). Amplitude and phase uncertainties were estimated as described in Appendix C of Rau et al. (2020).

Results of the HALS analysis are shown in Fig. B1 and identify the semi-diurnal characteristic of the ocean tides with only minor diurnal constituents. This pattern is retained in the groundwater response for BS3 and NY-10 (Fig. B1ab), but the principal diurnal solar constituent S_1 is amplified compared to the sea-level signal in the data observed at SN12/1, which indicates that parts of the spectral power present at this frequency must originate from another process (compare Sect. 3.5).

Figure B2 shows the amplitude ratio

$$R_\nu^A = \frac{A_\nu^{\mathrm{GW_c}}}{A_\nu^{\mathrm{GW}}}. \tag{B1}$$

between the amplitudes of tidal constituent ν in the observed (A_ν^{GW}) and corrected ($A_\nu^{\mathrm{GW_c}}$) groundwater time series for different sea-level memories m^{SL} between 1 h and 6 weeks. Uncertainties are shown as standard errors

$$\mathrm{SE}_{R_\nu^A} = |R_\nu^A| \sqrt{\left(\frac{\mathrm{SE}_{A_\nu^{\mathrm{GW_c}}}}{A_\nu^{\mathrm{GW_c}}}\right)^2 + \left(\frac{\mathrm{SE}_{A_\nu^{\mathrm{GW}}}}{A_\nu^{\mathrm{GW}}}\right)^2}, \tag{B2}$$

obtained by propagating amplitude uncertainties estimated using HALS.

Semi-diurnal constituents, like M_2 or S_2, are easily removed. A maximum lag of around 6 h suffices for reducing the amplitudes in BS3 and NY-10 below approximately 5 % to 10 % of their original values (Fig. B2ab). However, this is only the case for M_2 in SN12/1 (Fig. B2c). Diurnal constituents like O_1 require larger total memory of around 12 to 24 h to be reduced equally well (Fig. B2). However, a successful removal of O_1 can be assumed for larger amplitude ratios considering the smaller absolute amplitude in the observed signal compared to the semi-diurnal constituents (Fig. B1).

The S_1 tidal constituent is not removed from the groundwater signal, and is actually larger in the corrected groundwater signal than in the observed signal in BS3 and NY-10 (Fig. B2ab). Yet, this constituent has little overall effect due to its minor amplitude (Fig. B1ab). As noted in Sect. 3.5, corrected groundwater levels in SN12/1 contain daily signals from nearby production wells. Figure B2c shows that this diurnal pattern maps to S_1. The amplification of S_1 for BS3 and NY-10 in the

https://doi.org/10.5194/hess-2023-54
Preprint. Discussion started: 28 March 2023

corrected time series likely has the same origin and could be caused by removal of an interference between ocean tide's S_1 and the daily extraction signal in the observed data.

Code and data availability. Python scripts and data used in this work are available on Zenodo under https://doi.org/10.5281/zenodo.7647139 (Haehnel, 2023).

Author contributions. Patrick Haehnel – formal analysis, data curation, software, visualization, writing - original draft, writing - review & editing; Todd C. Rasmussen – methodology, formal analysis, supervision, writing - original draft, writing - review & editing; Gabriel C. Rau – conzeptualization, methodology, software, supervision, writing - original draft, writing - review & editing.

Competing interests. The authors declare that they have no conflict of interest.

Financial support. Research for this work was funded by the Federal Ministry of Education and Research of Germany (BMBF) through the project WAKOS (funding reference number 01LR2003E). The article processing charges of this open access publication were covered by the open access publication fund of the Carl von Ossietzky University Oldenburg, which is partly financed by the Scientific Library Services and Information Systems (LIS) programme of the German Research Foundation (DFG).

Acknowledgements. We thank the Stadtwerke Norderney (Municipal Works Norderney), especially O. Rass, for providing groundwater data and support as well as for approving the publication of this data in the Zenodo repository. Thanks to the Wasser- und Schifffahrtsverwaltung des Bundes (German Federal Waterways and Shipping Administration) as well as the Bundesamt für Gewässerschutz (German Federal Institute of Hydrology) for providing tide gauge data.

https://doi.org/10.5194/hess-2023-54
Preprint. Discussion started: 28 March 2023

Hydrology and Earth System Sciences
Discussions

References

Barlow, P. M.: Ground water in freshwater-saltwater environments of the Atlantic coast, vol. Circular 1262, US Geological Survey, Washington, D.C., 2003.

Boon, J. D.: Secrets of the Tide: Tide and Tidal Current Analysis and Applications, Storm Surges and Sea Level Trends, Woodhead Publishing, Cambridge, https://doi.org/10.1016/B978-1-904275-17-6.50011-2, 2011.

Butler Jr., J. J., Jin, W., Mohammed, G. A., and Reboulet, E. C.: New Insights from Well Responses to Fluctuations in Barometric Pressure, Groundwater, 49, 525–533, https://doi.org/10.1111/j.1745-6584.2010.00768.x, 2011.

DWD Climate Data Center (CDC): Historical daily station observations (temperature, pressure, precipitation, sunshine duration, etc.) for Norderney (station 3631), version v006, Deutscher Wetterdienst (DWD) [German Meteorological Service] [data set], https://opendata.dwd.de/climate_environment/CDC/observations_germany/climate/daily/kl/historical/, last access: 29 March 2021., 2021a.

DWD Climate Data Center (CDC): Historical hourly station observations of pressure and precipitation for Norderney (station 3631) from 1949 to 2020, version v21.3, Deutscher Wetterdienst (DWD) [German Meteorological Service] [data set], https://opendata.dwd.de/climate_environment/CDC/observations_germany/climate/hourly/pressure/historical/, last access: 1 October 2021., 2021b.

EuroGeographics and UN-FAO: Countries, 2020 - Administrative Units, 1:1 000 000, provided by Eurostat [data set], https://ec.europa.eu/eurostat/web/gisco/geodata/reference-data/administrative-units-statistical-units/countries, last access: 29 November 2021, 2020.

Falkland, A. and Custodio, E.: Hydrology and water resources of small islands: a practical guide, no. 49 in Studies and reports in hydrology, UNESCO, Paris, 1991.

Ferris, J. G.: Cyclic fluctuations of water level as a basis for determining aquifer transmissibility, USGS Unnumbered Series Note 1, US Geological Survey, Washington, D.C., https://doi.org/10.3133/70133368, 1952.

Furbish, D. J.: The response of water level in a well to a time series of atmospheric loading under confined conditions, Water Resourc. Res., 27, 557–568, https://doi.org/10.1029/90WR02775, 1991.

Gönnert, G.: Sturmfluten und Windstau in der Deutschen Bucht - Charakter, Veränderungen und Maximalwerte im 20. Jahrhundert, Die Küste, 67, 185–365, http://henry.baw.de/handle/20.500.11970/101500, 2003.

Haehnel, P.: Workflow, scripts, and data for technical note "Removing dynamic sea-level influences from groundwater-level measurements" (Version 1.0.0), Zenodo, https://doi.org/10.5281/zenodo.7647139, 2023.

Haehnel, P., Freund, H., Greskowiak, J., and Massmann, G.: Development of a three-dimensional hydrogeological model for the island of Norderney (Germany) using GemPy, Geosci. Data J., XX, XX, under review.

Hayes, M. O.: Barrier Island Morphology as a Function of Tidal and Wave Regime, in: Barrier Islands from the Gulf of St. Lawrence to the Gulf of Mexico, edited by Leatherman, S. P., pp. 1–29, Academic Press, New York, 1979.

Holt, T., Greskowiak, J., Seibert, S. L., and Massmann, G.: Modeling the Evolution of a Freshwater Lens under Highly Dynamic Conditions on a Currently Developing Barrier Island, Geofluids, 2019, 9484 657, https://doi.org/10.1155/2019/9484657, 2019.

Houben, G. J., Koeniger, P., and Sültenfuß, J.: Freshwater lenses as archive of climate, groundwater recharge, and hydrochemical evolution: Insights from depth-specific water isotope analysis and age determination on the island of Langeoog, Germany, Water Resourc. Res., 50, 8227–8239, 2014.

Jiao, J. J. and Post, V. E. A.: Coastal Hydrogeology, Cambridge University Press, Cambridge, https://doi.org/10.1017/9781139344142, 2019.

Karle, M., Bungenstock, F., and Wehrmann, A.: Holocene coastal landscape development in response to rising sea level in the Central Wadden Sea coastal region, Neth. J. Geosci., 100, e12, https://doi.org/10.1017/njg.2021.10, 2021.

https://doi.org/10.5194/hess-2023-54
Preprint. Discussion started: 28 March 2023

Hydrology and Earth System Sciences
Discussions

Koeniger, P., Gaj, M., Beyer, M., and Himmelsbach, T.: Review on soil water isotope-based groundwater recharge estimations, Hydrol. Process., 30, 2817–2834, https://doi.org/10.1002/hyp.10775, 2016.

Li, L., Cartwright, N., Nielsen, P., and Lockington, D.: Response of Coastal Groundwater Table to Offshore Storms, Cina Ocean Eng., 18, 423–431, 2004.

McMillan, T. C., Rau, G. C., Timms, W. A., and Andersen, M. S.: Utilizing the Impact of Earth and Atmospheric Tides on Groundwater Systems: A Review Reveals the Future Potential, Rev. Geophys., 57, 281–315, https://doi.org/10.1029/2018RG000630, 2019.

Naumann, K.: Eine hydrogeologische Systemanalyse von Süßwasserlinsen als Grundlage einer umweltschonenden Grundwasserbewirtschaftung, Ph.D. thesis, Technischen Universität Carolo-Wilhelmina zu Braunschweig, Braunschweig, 2005.

Niedersächsischer Landesbetrieb für Wasserwirtschaft, Küsten- und Naturschutz (NLWKN) [Lower Saxony State Agency for Water Management, Coastal and Nature Conservation]: Dedicated dikes in Lower Saxony [data set], https://geoportal.geodaten.niedersachsen.de/harvest/srv/ger/catalog.search#/metadata/8A90C8B8-68D0-485C-9950-8964E6921244, last access: 28 April 2022, 2021.

Nielsen, P.: Tidal dynamics of the water table in beaches, Water Resourc. Res., 26, 2127–2134, https://doi.org/10.1029/WR026i009p02127, 1990.

Olsthoorn, T. N.: Do a Bit More with Convolution, Groundwater, 46, 13–22, https://doi.org/10.1111/j.1745-6584.2007.00342.x, 2008.

Patton, A. M., Rau, G. C., Cleall, P. J., and Cuthbert, M. O.: Hydro-geomechanical characterisation of a coastal urban aquifer using multiscalar time and frequency domain groundwater-level responses, Hydrogeol. J., 29, 2751–2771, https://doi.org/10.1007/s10040-021-02400-5, 2021.

Petersen, J., Pott, R., Janiesch, P., and Wolff, J.: Umweltverträgliche Grundwasserbewirtschaftung in hydrologisch und ökologisch sensiblen Bereichen der Nordseeküste, Husum Druck- und Verlagsgesellschaft mbH u. Co. KG., Husum, 2003.

Post, V. E. A., Houben, G. J., and van Engelen, J.: What is the Ghijben-Herzberg principle and who formulated it?, Hydrogeol. J., 26, 1801–1807, https://doi.org/10.1007/s10040-018-1796-0, 2018.

Post, V. E. A., Zhou, T., Neukum, C., Koeniger, P., Houben, G. J., Lamparter, A., and Šimůnek, J.: Estimation of groundwater recharge rates using soil-water isotope profiles: A case study of two contrasting dune types on Langeoog Island, Germany, Hydrogeol. J., 30, 797—812, https://doi.org/10.1007/s10040-022-02471-y, 2022.

Rasmussen, T. C. and Crawford, L. A.: Identifying and Removing Barometric Pressure Effects in Confined and Unconfined Aquifers, Groundwater, 35, 502–511, https://doi.org/10.1111/j.1745-6584.1997.tb00111.x, 1997.

Rasmussen, T. C. and Mote, T. L.: Monitoring Surface and Subsurface Water Storage Using Confined Aquifer Water Levels at the Savannah River Site, USA, Vadose Zone J., 6, 327–335, https://doi.org/10.2136/vzj2006.0049, 2007.

Rau, G. C., Cuthbert, M. O., Acworth, R. I., and Blum, P.: Technical note: Disentangling the groundwater response to Earth and atmospheric tides to improve subsurface characterisation, Hydrol. and Earth Syst. Sc., 24, 6033–6046, https://doi.org/10.5194/hess-24-6033-2020, 2020.

Rojstaczer, S. and Riley, F. S.: Response of the water level in a well to Earth tides and atmospheric loading under unconfined conditions, Water Resourc. Res., 26, 1803–1817, https://doi.org/10.1029/WR026i008p01803, 1990.

Röper, T., Kröger, K. F., Meyer, H., Sültenfuss, J., Greskowiak, J., and Massmann, G.: Groundwater ages, recharge conditions and hydrochemical evolution of a barrier island freshwater lens (Spiekeroog, Northern Germany), J. Hydrol., 454-455, 173–186, https://doi.org/10.1016/j.jhydrol.2012.06.011, 2012.

https://doi.org/10.5194/hess-2023-54
Preprint. Discussion started: 28 March 2023

Schaumann, R. M., Capperucci, R. M., Bungenstock, F., McCann, T., Enters, D., Wehrmann, A., and Bartholomä, A.: The Middle Pleistocene to early Holocene subsurface geology of the Norderney tidal basin: new insights from core data and high-resolution sub-bottom profiling (Central Wadden Sea, southern North Sea), Neth. J. Geosci., 100, e15, https://doi.org/10.1017/njg.2021.3, 2021.

Schweizer, D., Ried, V., Rau, G. C., Tuck, J. E., and Stoica, P.: Comparing Methods and Defining Practical Requirements for Extracting Harmonic Tidal Components from Groundwater Level Measurements, Math. Geosci., 53, 1147–1169, https://doi.org/10.1007/s11004-020-09915-9, 2021.

Shirahata, K., Yoshimoto, S., Tsuchihara, T., and Ishida, S.: Digital Filters to Eliminate or Separate Tidal Components in Groundwater Observation Time-Series Data, JARG-Jpn. Agr. Res. Q., 50, 241–252, https://doi.org/10.6090/jarq.50.241, 2016.

Sievers, J., Rubel, M., and Milbradt, P.: EasyGSH-DB: Bathymetrie (2016), Bundesanstalt für Wasserbau (BAW) [Federal Waterways Engineering and Research Institute] [data set], https://doi.org/10.48437/02.2020.K2.7000.0002, 2020.

Spane, F. A.: Considering barometric pressure in groundwater flow investigations, Water Resources Research, 38, 14–1–14–18, https://doi.org/https://doi.org/10.1029/2001WR000701, 2002.

Spane, F. A. and Mackley, R. D.: Removal of River-Stage Fluctuations from Well Response Using Multiple Regression, Ground Water, 49, 794–807, https://doi.org/10.1111/j.1745-6584.2010.00780.x, 2011.

Stadtwerke Norderney [Municipal Works Norderney]: Groundwater time series of the Norderney municipal works from 2016 to 2020 (1 hour) [data set], 2021.

Stadtwerke Norderney [Municipal works Norderney]: Groundwater database of the Norderney municipal works [data set], 2021.

Stadtwerke Norderney [Municipal Works Norderney]: Hourly groundwater abstraction volumes of water works I and II on Norderney from 13 to 20 November 2022 [data set], 2023.

Streif, H.: Das ostfriesische Küstengebiet. Nordsee, Inseln, Watten und Marschen, in: Sammlung geologischer Führer, edited by Gwinner, M. P., vol. 57, Gebrüder Borntraeger, Stuttgart, Germany, 2nd fully revised edn., 1990.

Stuyfzand, P. J.: Observations and analytical modeling of freshwater and rainwater lenses in coastal dune systems, J. Coast. Conserv., 21, 577–593, https://doi.org/10.1007/s11852-016-0456-6, 2017.

Toll, N. J. and Rasmussen, T. C.: Removal of Barometric Pressure Effects and Earth Tides from Observed Water Levels, Groundwater, 45, 101–105, https://doi.org/10.1111/j.1745-6584.2006.00254.x, 2007.

Underwood, M. R., Peterson, F. L., and Voss, C. I.: Groundwater lens dynamics of Atoll Islands, Water Resourc. Res., 28, 2889–2902, https://doi.org/10.1029/92wr01723, 1992.

Wasserstraßen- und Schifffahrtsamt Ems-Nordsee (WSA Ems-Nordsee) [Waterways and Shipping Authority Ems-North Sea]: High and low water time series from tide gauge Norderney Riffgat from 1963 to 2021, provided by Bundesanstalt für Gewässerkunde (BfG) [German Federal Institute of Hydrology] [data set], 2021.

Wasserstraßen- und Schifffahrtsverwaltung des Bundes (WSV) [Federal Waterways and Shipping Administration]: Sea level time series data for tide gauge Norderney Riffgat from 1999 to 2021 (1 min), provided by Bundesanstalt für Gewässerkunde (BfG) [German Federal Institute of Hydrology] [data set], 2021.

White, I. and Falkland, T.: Management of freshwater lenses on small Pacific islands, Hydrogeol. J., 18, 227–246, https://doi.org/10.1007/s10040-009-0525-0, 2009.